ANNALS of the ORADEA UNIVERSITY.

Fascicle of Management and Technological Engineering, Volume VII (XVII), 2008

SIMULATION OF GEAR RACK GENERATION OF INVOLUTE SPUR GEARS

Stelian ALACI, Dumitru AMARANDEI,
Florina-Carmen CIORNEI, Simion PĂTRAŞ-CICEU
„Ştefan cel Mare" University, Department of Mechanical Engineering, Suceava
e-mail: stalaci@yahoo.com

Keywords: involute teeth, rack generation, tip relief, undercutting

Abstract: The paper presents the results of a program developed with the MATHCAD application that allows the simulation of involute teeth gear generation by rack generation. The specific aspects regarding teeth manufacturing are graphically evidenced: undercutting, tip relief and the effect of rack cutter displacement upon manufacturing.

1. INTRODUCTION

Involute teeth gears are manufactured by two main methods [1]: by forming the gear teeth by using milling and by rack generation. The first method uses an involute forming cutter which has the profile of the space between the teeth and has disadvantages as: reduced precision, expensive cutters and gears with addendum modification can not be manufactured.

These inconvenients are eliminated using rack generation, a method based on the envelope of successive positions set of a cutting rack having a well defined and controlled motion. This method assumes a special cutting tool and it applies specially to mass and large series production.

2. THEORETICAL ASPECTS

By rack generating manufacturing, the gear results as an envelope of successive positions of the tool. The tool is a teethed element with cutting properties.

Next, we assume that the gears are manufactured using a tool with rack profile. Its profile is conjugated with the reference rack having standard shape and dimensions. Figure 1 shows the profile of the cutting rack. One can observe cutting edges round the teeth boundaries, the tip radius of $\rho_0 = mc_0^* /(1-\sin\alpha_0)$ where *m* is the tool modulus, $c_0^* = 0.25$ is the radial clearance coefficient and $\alpha_0 = 20^o$ is the angle between the reference rack profile and the normal to the direction of tool movement direction. Δ_{w_0} is the straight line of tool movement, line that rolls without friction over the pitch circle. The rolling straight line has a displacement equal with the quantity $X = mx$ with respect to the reference straight line of the gear (along which the tooth has the same thickness as the width space) and x is the addendum modification of the gear.

One can observe that the pitch circle C_d of the gear and the straight line Δ_{w_0} are the centrodes of relative movement during manufacturing.

The equations of the reference rack profile are given in **Appendix**.

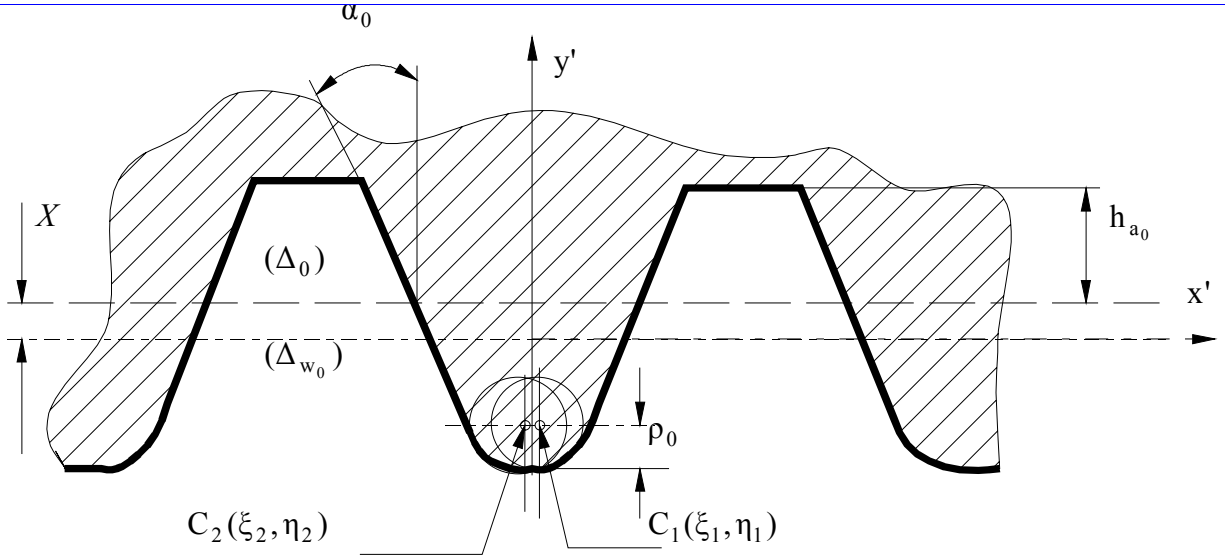

Fig.1. Rack generator

Handra-Luca, [2], presents the equations of the fillet profile from the bottom land by imposing the condition that both the tool profile and the gear profile from non-involute region should obey the fundamental law of toothed gearing. In the present paper the equations of the fillet profile are deduced from the property of the profile to envelop the tool tooth. In the coordinate system $Ox'y'$ the Ox' axis is directed along the rolling straight line of the tool (cutting centrode) (Δ_{w_0}) and the $O'y'$ is the symmetry axis for one tooth of the tool, Fig. 2, centres coordinates $C_1(\xi_1,\eta_1)$ and $C_2(\xi_2,\eta_2)$ of the circles that fillet the tip of the tooth are:

$$C_1\begin{cases}\xi_{1,2}=\left[\pi/4-h^*_{a_0}\tan(\alpha_0)-\rho_0\cos(\alpha_0)\right]m,\\ \eta_{1,2}=[h^*_{a_0}-x-\rho_0\sin(\alpha_0)]m,\end{cases} \tag{1}$$

$$C_2\begin{cases}\xi_{1,2}=-\left[\pi/4-h^*_{a_0}\tan(\alpha_0)-\rho_0\cos(\alpha_0)\right]m,\\ \eta_{1,2}=[h^*_{a_0}-x-\rho_0\sin(\alpha_0)]m.\end{cases} \tag{2}$$

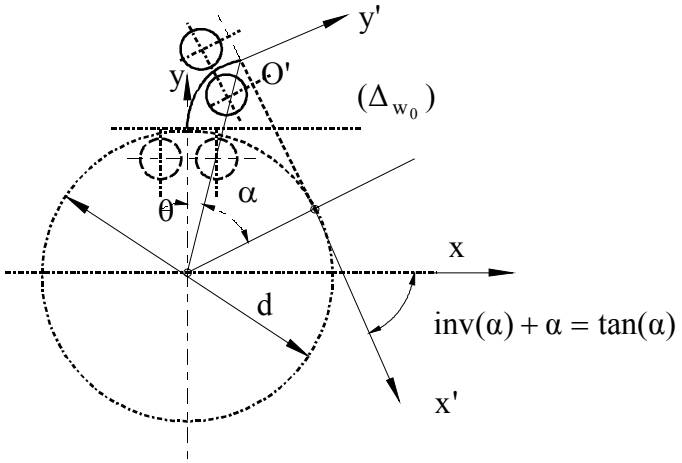

Fig. 2. Reference system used in the paper

During rolling of axis Ox', (Δ_w), over the pitch circle (c_d) the centres of the circles describe lengthened or shortened involutes, as the centres of fillet circles are placed underneath or on top of straight line (Δ_{w_0}), respectively. In coordinate system Oxy, fixed with the gear, Fig. 2, the coordinates of the points C_1 and C_2 become:

$$\begin{cases} x_{0_{1,2}} = \dfrac{mz}{2\cos(\alpha)} \sin[inv(\alpha)] + \xi_{1,2}\cos[\tan(\alpha)] + \eta_{1,2}\sin[\tan(\alpha)] \\ y_{0_{1,2}} = \dfrac{mz}{2\cos(\alpha)} \cos[inv(\alpha)] - \xi_{1,2}\cos[\tan(\alpha)] + \eta_{1,2}\cos[\tan(\alpha)], \end{cases} \tag{3}$$

The equations of the envelope of curves (3) is found from the system:

$$\begin{cases} f(x,y,\alpha) = [x - x_{0_{1,2}}]^2 + [y - y_{0_{1,2}}]^2 - \rho_0^2 = 0, \\ \dfrac{\partial f(x,y,\alpha)}{\partial \alpha} = 0. \end{cases} \tag{4}$$

The concrete form of system (4) is

$$\begin{cases} x_{1,2} = x_{01,2} \pm \dfrac{\dfrac{\partial x_{01,2}}{\partial \alpha}}{\sqrt{\left(\dfrac{\partial x_{01,2}}{\partial \alpha}\right)^2 + \left(\dfrac{\partial y_{01,2}}{\partial \alpha}\right)^2}} \rho_0, \\ y_{1,2} = y_{01,2} \mp \dfrac{\dfrac{\partial x_{01,2}}{\partial \alpha}}{\sqrt{\left(\dfrac{\partial x_{01,2}}{\partial \alpha}\right)^2 + \left(\dfrac{\partial y_{01,2}}{\partial \alpha}\right)^2}} \rho_0. \end{cases} \tag{5}$$

After computing the calculus from relation (5) the parametric equations of the envelopes are obtained:

$$\begin{cases} x(\alpha) = \dfrac{m\,z}{2\cos(\alpha)} \sin[inv(\alpha)] + \xi_{1,2}\cos[\tan(\alpha)] + \eta_{1,2}\sin[\tan(\alpha)]... \\ \pm \dfrac{mz\cos[inv(\alpha)]\sin(\alpha) - 2\{\xi_{1,2}\cos[\tan(\alpha)] + \eta_{1,2}\sin[\tan(\alpha)]\}\cos(\alpha)}{\sqrt{[mz\sin(\alpha) + 2\cos(\alpha)\xi_{1,2}]^2 + 4\cos(\alpha)^2\eta_{1,2}^2}} \dfrac{\rho_0}{m}, \\ y(\alpha) = \dfrac{m\,z}{2\cos(\alpha)} \cos[inv(\alpha)] + \xi_{1,2}\sin[\tan(\alpha)] + \eta_{1,2}\cos[\tan(\alpha)]... \\ \mp \dfrac{mz\sin[inv(\alpha)]\sin(\alpha) - 2\{\xi_{1,2}\cos[\tan(\alpha)] + \eta_{1,2}\sin[\tan(\alpha)]\}\cos(\alpha)}{\sqrt{[mz\sin(\alpha) + 2\cos(\alpha)\xi_{1,2}]^2 + 4\cos(\alpha)^2\eta_{1,2}^2}} \dfrac{\rho_0}{m}. \end{cases} \tag{6}$$

Figure 3 presents the involutes described by the centres of the fillet circles, the two families of circles with ρ_0 radius, with the centre placed on these involutes. Using equations (6), the envelopes of the circles families were represented. As it can be seen from Fig. 3, each of the two families of circles admits two envelope curves from which only one is tooth profile. In Fig. 3, the dash lines are used in representing the coiled involutes described by the centres of the two circles. After graphical drawing, one can eliminate the curves that don't fit in the tooth profile.

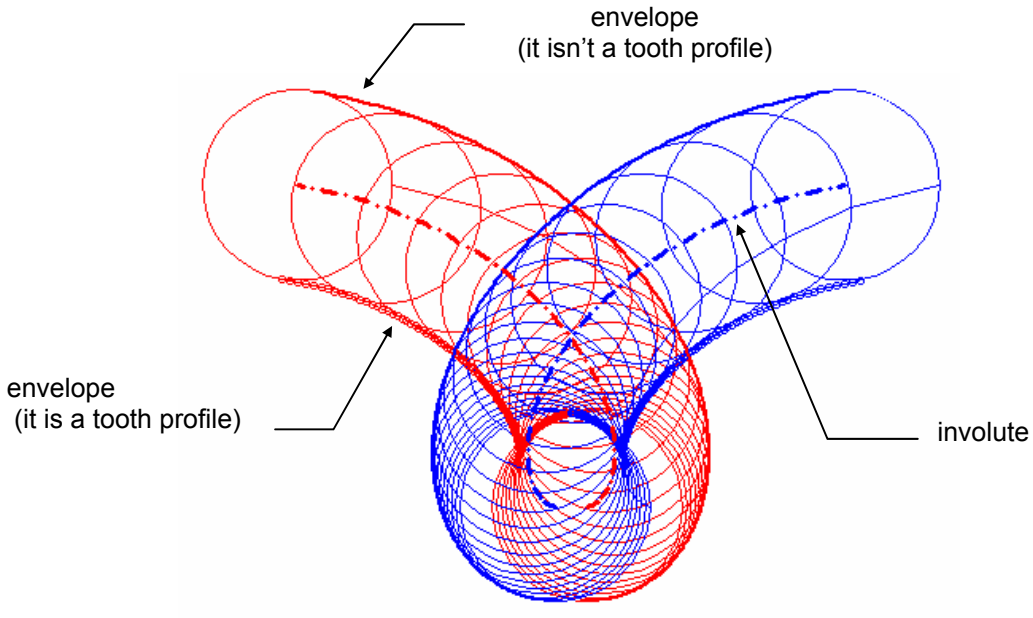

Fig. 3. Involutes described by the centres of the fillet circles

In addition to the undercutting effect, when the tooth of the cutting tool effectively incises the tooth dedendum, another negative effect is the tip relief. The phenomenon consists in the fact the tooth thickness on addendum circle becomes zero or negative.

3. RESULTS

Using rolling condition between the pitch circle of gear blank and the rolling straight line of the cutting rack, the teeth profiles for different situations were obtained, underlying the mentioned aspects. Figures 4-7 present the shapes of teeth of some gears obtained with the program. With solid line the addendum and dedendum circles are traced. The base circle is drawn with dash line. In Figures 4, 6 and 7 the teeth are undercut and in Figure 7 the tip relief is present. Generally, the two phenomena are in contradiction, but, for small teeth number, $z \leq 8$ they can both appear, as seen in Figure 8.

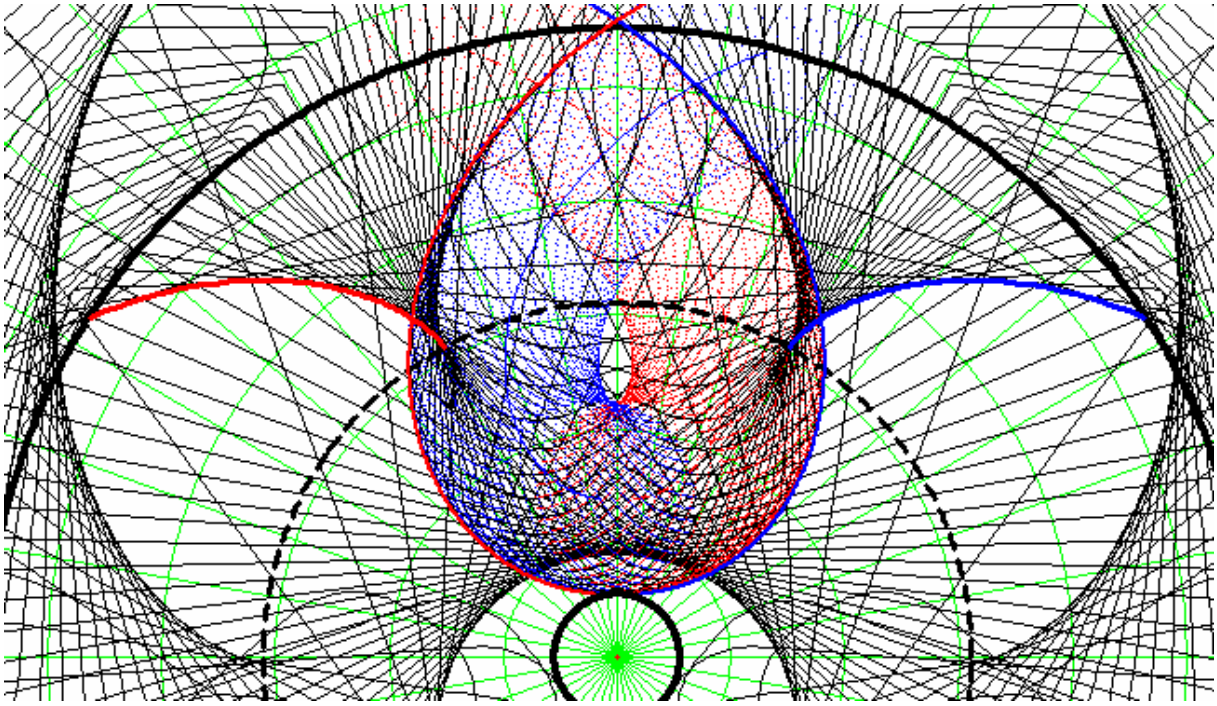

Fig.4. Undercut tooth

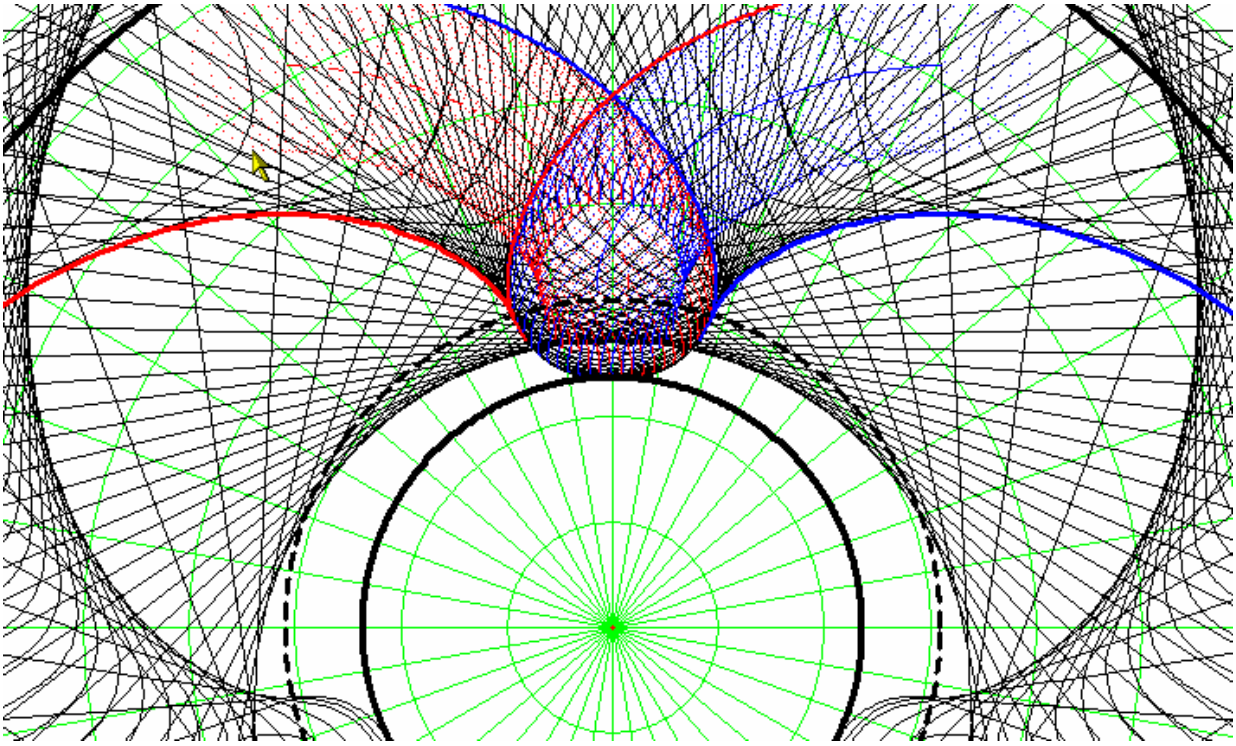

Fig. 5. Normal tooth

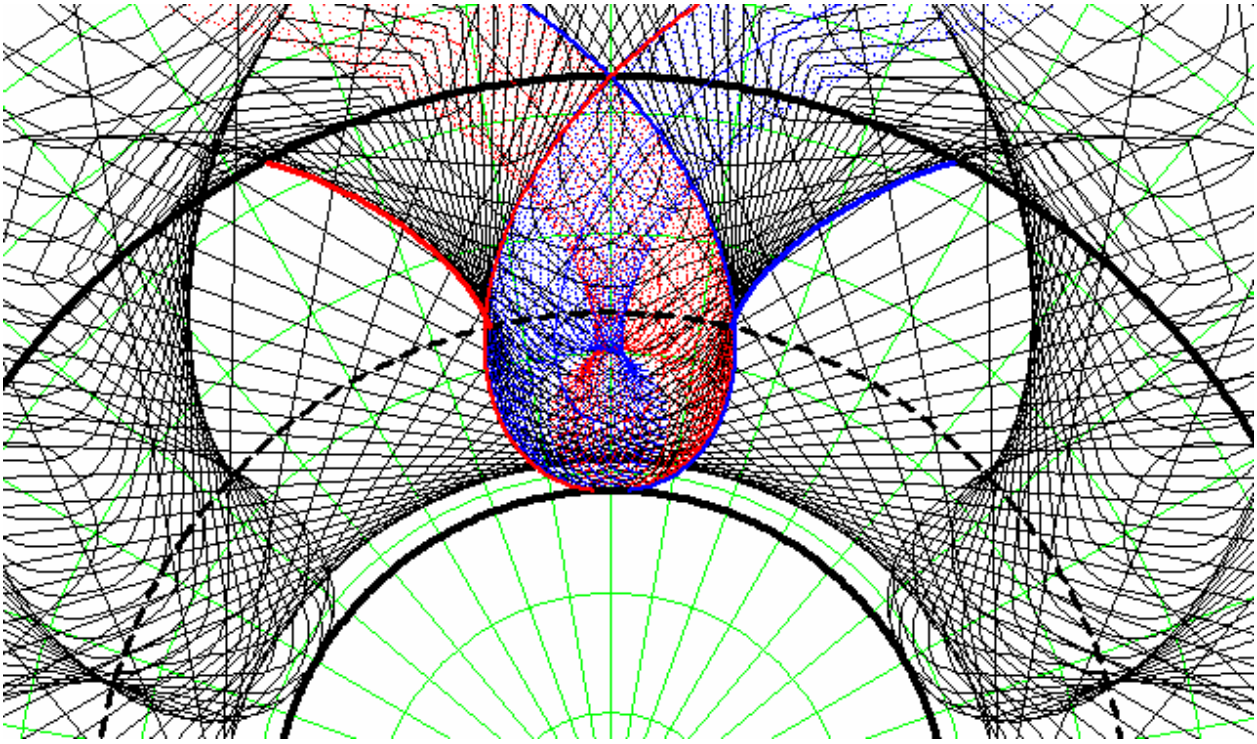

Fig. 6. Undercut tooth

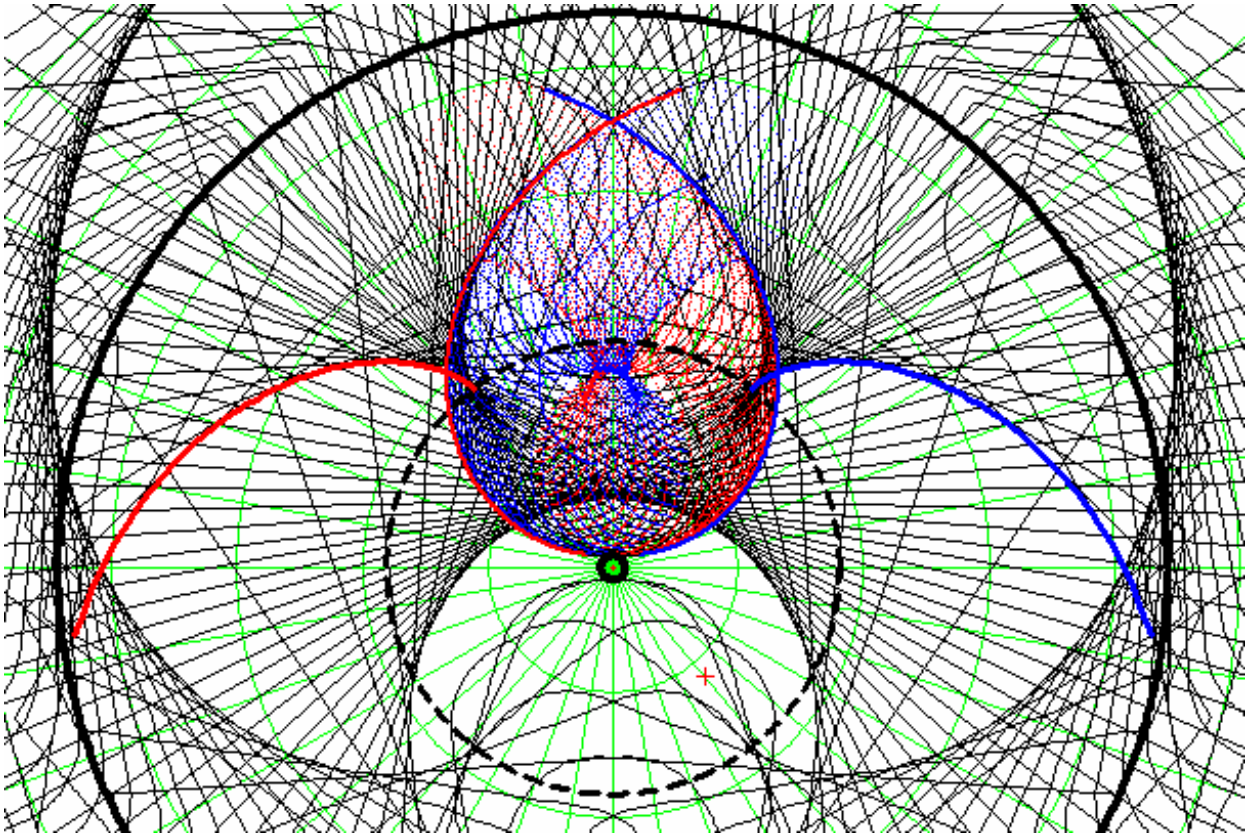

Fig. 7. Tip relief and undercutting

The undercutting radius can be calculated by solving the system:

$$\begin{cases} \dfrac{m\,z}{2\cos(\alpha')}\sin[inv(\alpha')] + \xi_2\cos[\tan(\alpha')] + \eta_2\sin[\tan(\alpha')]... \\ + \dfrac{mz\cos[inv(\alpha')]\sin(\alpha') - 2\{\xi_2\cos[\tan(\alpha')] + \eta_2\sin[\tan(\alpha')]\}\cos(\alpha')}{\sqrt{[mz\sin(\alpha') + 2\cos(\alpha')\xi_2]^2 + 4\cos(\alpha')^2\eta_2^2}}\rho_0 = \\ = r(\alpha'')\cos\left[\dfrac{\pi}{2} + \dfrac{\psi(\alpha'')}{2}\right], \\ \dfrac{m\,z}{2\cos(\alpha')}\cos[inv(\alpha')] + \xi_2\sin[\tan(\alpha')] + \eta_2\cos[\tan(\alpha')]... \\ - \dfrac{mz\sin[inv(\alpha')]\sin(\alpha) - 2\{\xi_1\cos[\tan(\alpha')] + \eta_2\sin[\tan(\alpha')]\}\cos(\alpha')}{\sqrt{[mz\sin(\alpha') + 2\cos(\alpha')\xi_2]^2 + 4\cos(\alpha')^2\eta_2^2}}\rho_0 = \\ = r(\alpha'')\sin\left[\dfrac{\pi}{2} + \dfrac{\psi(\alpha'')}{2}\right], \end{cases} \tag{7}$$

where:

$$r(\alpha'') = \frac{r_b}{\cos(\alpha'')} = \frac{mz\cos(\alpha_0)}{2\cos(\alpha'')},$$

$$\psi(\alpha'') = \frac{\pi}{2z} - 2\frac{x}{z}\tan(\alpha_0) + inv(\alpha'') - inv(\alpha_0). \tag{8}$$

The system (7) results from the condition that an involute generated using a base circle of radius r_b intersects the fillet profile described by equations (6). The unknowns of the system are the pressure angles α' and α''. The system requires a numerical solving method as it is a transcendental one. The system presents real solutions only when the addendum straight line of the cutting rack intersects the pressure line outside the tangency points of pressure line with the base circles. Figure 8 presents an undercut tooth for which the circle of radius r_S (in dot line) is drawn obtained by solving the system (8). For the calculus of r_u, radius that bounds the involute profile and the non-involute one, the relation given by Duca, [3], is used:

$$r_u = OA = \sqrt{OK^2 + KC^2} = \sqrt{OK^2 + (KC - AC)^2} =$$

$$= \sqrt{r_b^2 + \left[r_b\tan(\alpha_0) - \frac{h_{a_0}^* - x}{\sin(\alpha_0)}m\right]^2} = m\sqrt{\left[\frac{z\cos(\alpha_0)}{2}\right]^2 + \left[\frac{z\sin(\alpha_0)}{2} - \frac{h_{a_0}^* - x}{\sin(\alpha_0)}\right]^2}. \tag{9}$$

The relation (9) agrees with the relations given by Maroş, [4], Handra-Luca, [2]. One can observe that the relation for the bound radius given in standard STAS 12222, [5], is not correct.

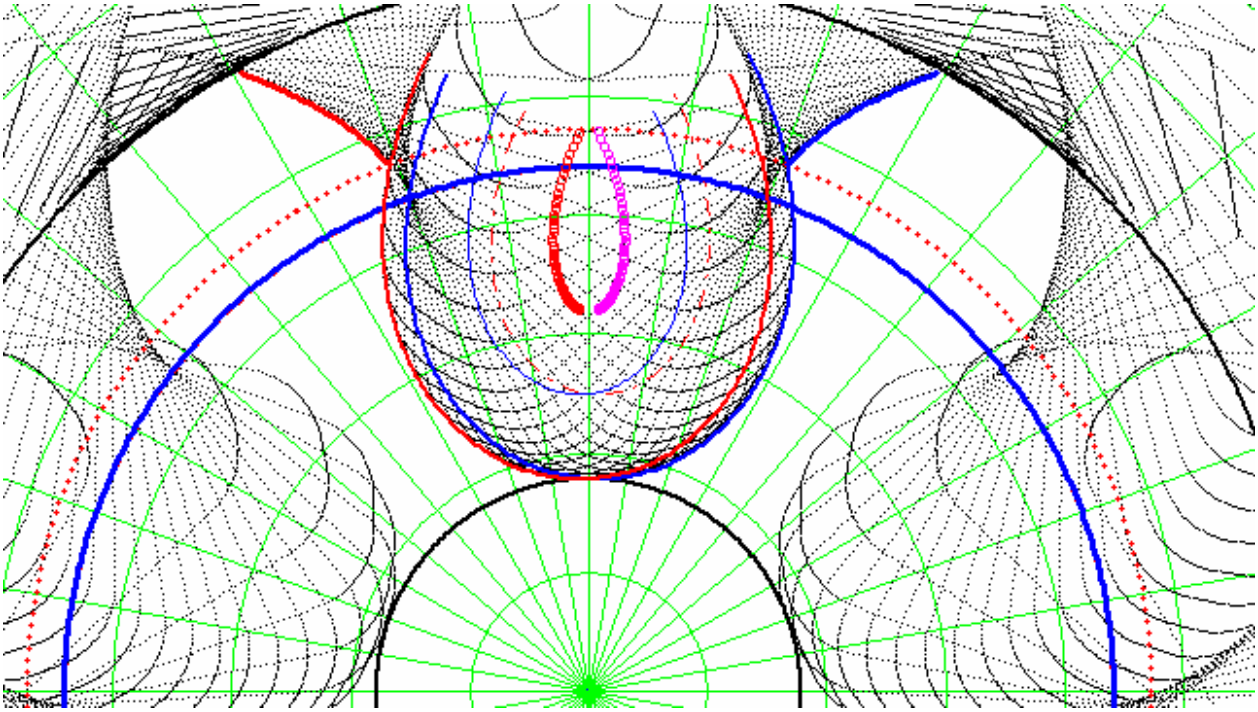

Fig. 8. Plot of the undercutting circle (dot line)

Also, the relation (9) applies only when

$$\frac{z\,sin(\alpha_0)}{2} - \frac{h_{a_0}^* - x}{sin(\alpha_0)} \geq 0\,. \tag{10}$$

It is obvious that the relation (10) represents the condition to avoid undercutting, [4].

CONCLUSIONS

The paper evidences the effects as tip relief and undercutting of spur gear during rack generation.

The effects of displacement of rack cutter upon these two phenomena are presented.

Analytic relations of fillet profile are obtained and the system for the calculus of undercutting radius is deduced, highlighting the undercutting conditions.

Acknowledgement
The results of this paper were found in the course of an investigation supported by CENVITMAR-CEEX contract number 292/13.09.2006.

REFERENCES

[1]. Uicker, J.J.jr., Pennock, G.R., Shigley, J.E., *Theory of Machines and Mechanisms*, Oxford University Press, 2003
[2] Handra-Luca, V. *Introducere în teoria mecanismelor*, editura Dacia, Cluj-Napoca, 1982:
[3] Duca, C., *Mecanisme,* Institutul Politehnic Iasi, 1983;
[4] Maroş, D., ş.a., *Teoria mecanismelor şi maşinilor. Cinematica roților dințate*, Ed. Tehnică, Bucureşti, 1958;
[5] *** STAS 12222 *Angrenaje paralele cilindrice exterioare cu danturi drepte în evolventă. Calculul geometric şi cinematic.*

Appendix

The equation of rack cutting with respect to the reference straight line

$$
f(t)=\begin{cases}
-(h_{a_0}^{*}+c_0^{*}),\ 0\le t<\dfrac{\pi}{4}-\dfrac{\rho_0}{m}-h_{a_0}^{*}\tan(\alpha_0) \\
-h_{a_0}^{*}+\dfrac{c_0^{*}\sin(\alpha_0)}{1-\sin(\alpha_0)}-\sqrt{\left(\dfrac{\rho_0}{m}\right)^2-\left[t-\left(\dfrac{\pi}{4}-\dfrac{c_0^{*}\sin(\alpha_0)}{1-\sin(\alpha_0)}-h_{a_0}^{*}\tan(\alpha_0)\right)\right]^2},\ \dfrac{\pi}{4}-\dfrac{\rho_0}{m}-h_{a_0}^{*}\tan(\alpha_0)\le t<\dfrac{\pi}{4}-h_{a_0}^{*}\tan(\alpha_0) \\
-h_{a_0}^{*}+\dfrac{1}{h_{a_0}^{*}\tan(\alpha_0)}\left[t-\dfrac{\pi}{4}+h_{a_0}^{*}\tan(\alpha_0)\right],\ \dfrac{\pi}{4}-h_{a_0}^{*}\tan(\alpha_0)\le t<\dfrac{\pi}{4}+h_{a_0}^{*}\tan(\alpha_0) \\
h_{a_0}^{*},\ \dfrac{\pi}{4}+h_{a_0}^{*}\tan(\alpha_0)\le t<\dfrac{3\cdot\pi}{4}-h_{a_0}^{*}\tan(\alpha_0) \\
h_{a_0}^{*}-\dfrac{1}{h_{a_0}^{*}\tan(\alpha_0)}\left[t-\dfrac{3\cdot\pi}{4}+h_{a_0}^{*}\tan(\alpha_0)\right],\ \dfrac{3\cdot\pi}{4}-h_{a_0}^{*}\tan(\alpha_0)\le t<\dfrac{3\cdot\pi}{4}+h_{a_0}^{*}\tan(\alpha_0) \\
-h_{a_0}^{*}+\dfrac{c_0^{*}\sin(\alpha_0)}{1-\sin(\alpha_0)}-\sqrt{\left(\dfrac{\rho_0}{m}\right)^2-\left[t-\dfrac{3\cdot\pi}{4}+h_{a_0}^{*}\tan(\alpha_0)+\dfrac{\rho_0}{m}\cos(\alpha_0)\right]^2},\ \dfrac{3\cdot\pi}{4}+h_{a_0}^{*}\tan(\alpha_0)\le t<\dfrac{3\cdot\pi}{4}+h_{a_0}^{*}\tan(\alpha_0)+\dfrac{\rho_0}{m}\cos(\alpha_0) \\
-(h_{a_0}^{*}+c_0^{*}),\ \dfrac{3\cdot\pi}{4}+h_{a_0}^{*}\tan(\alpha_0)+\dfrac{\rho_0}{m}\cos(\alpha_0)\le t\le\pi
\end{cases}
$$